AD-A117 525 UTAH UNIV SALT LAKE CITY DEPT OF BIOENGINEERING F/G 9/1
EQUILIBRIUM NOISE IN ION SELECTIVE FIELD EFFECT TRANSISTORS.(U)
JUL 82 A M HAEMMERLI, J JANATA, J J BROPHY N00014-81-K-0664
UNCLASSIFIED TR-1 NL

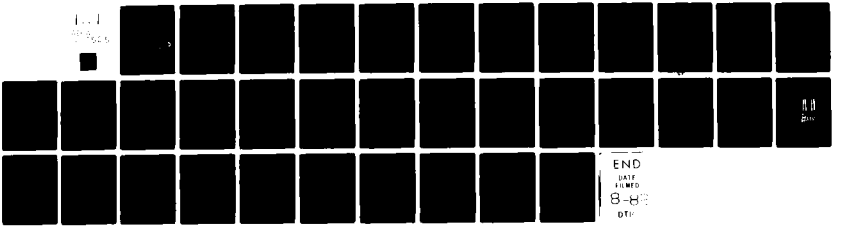

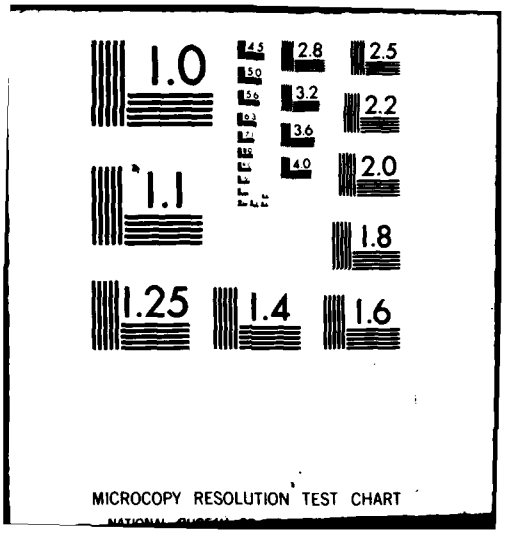
1.0
1.1
1.25
1.4
1.6
1.8
2.0
2.2
2.5
2.8
3.2
3.6
4.0
4.5
5.0
5.6
6.3
MICROCOPY RESOLUTION TEST CHART

OFFICE OF NAVAL RESEARCH

Contract N00014-81-K-0664

Task No. NR 051-778/5-29-82 (472)

TECHNICAL REPORT NO. 1

EQUILIBRIUM NOISE IN ION SELECTIVE FIELD EFFECT TRANSISTORS

by

Andre M. Haemmerli, Jiri Janata*, and James J. Brophy

Prepared for publication in the

Journal of Electrochemical Society

Department of Bioengineering
University of Utah
Salt Lake City, Utah 84112

July 21, 1982

SECURITY CLASSIFICATION OF THIS PAGE (When Data Entered)

REPORT DOCUMENTATION PAGE

READ INSTRUCTIONS BEFORE COMPLETING FORM

1. REPORT NUMBER: Technical Report No. 1	2. GOVT ACCESSION NO.: AD-A117525
3. RECIPIENT'S CATALOG NUMBER:	
4. TITLE (and Subtitle): Equilibrium Noise in Ion Selective Field Effect Transistors	5. TYPE OF REPORT & PERIOD COVERED: Interim Technical Report
	6. PERFORMING ORG. REPORT NUMBER:
7. AUTHOR(s): Andre M. Haemmerli, Jiri Janata, and James J. Brophy	8. CONTRACT OR GRANT NUMBER(s): N00014-81-K-0664
9. PERFORMING ORGANIZATION NAME AND ADDRESS: Department of Bioengineering, University of Utah, Salt Lake City, Utah 84112	10. PROGRAM ELEMENT, PROJECT, TASK AREA & WORK UNIT NUMBERS: NR 051-77815-29-81 (472)
11. CONTROLLING OFFICE NAME AND ADDRESS: Elmer G. Keith, ONR, University of California, 239 Campbell Ave., Berkeley, CA 94720	12. REPORT DATE: 21 July 1982
	13. NUMBER OF PAGES: 30
14. MONITORING AGENCY NAME & ADDRESS(if different from Controlling Office)	15. SECURITY CLASS. (of this report): Unclassified
	15a. DECLASSIFICATION/DOWNGRADING SCHEDULE

16. DISTRIBUTION STATEMENT (of this Report)

Approved for public release: distribution unlimited

17. DISTRIBUTION STATEMENT (of the abstract entered in Block 20, if different from Report)

18. SUPPLEMENTARY NOTES

Prepared for publication in Journal of Electrochemical Society

19. KEY WORDS (Continue on reverse side if necessary and identify by block number)

Ion Selective Field Effect Transistors; Equilibrium Noise Analysis; Ion Selective Membranes

20. ABSTRACT (Continue on reverse side if necessary and identify by block number)

It has been shown that noise which is in excess of the semiconductor device noise can be identified with the electrochemical processes taking place in ISFETs. The frequency analysis of this noise yields information about interfacial capacitance and exchange current density at the membrane/solution interface. These parameters have been evaluated for several ion-selective membranes.

DD FORM 1 JAN 73 1473 EDITION OF 1 NOV 65 IS OBSOLETE
S/N 0102-LF-014-6601

SECURITY CLASSIFICATION OF THIS PAGE (When Data Entered)

EQUILIBRIUM NOISE IN ION SELECTIVE FIELD EFFECT TRANSISTORS

André Haemmerli, Jiří Janata, and James J. Brophy

Department of Bioengineering

University of Utah

Salt Lake City, Utah 84112 U.S.A.

ABSTRACT

Noise spectra of the drain current of ion selective field effect transistors (ISFETs) in equilibrium were measured. The spectra differ from one type of ISFET to the other. The ionic activity in solution does not modify perceptibly the noise level for any of the various types of ISFETs. Computer assisted modeling is used to fit experimental data and to assign an equivalent electrical circuit to the electrochemical system. The overall response time of the system is shown to depend on the input capacitance of the electrometer.

INTRODUCTION

A considerable amount of research has been devoted to the ion selective field effect transistor (ISFET), and the subject has been recently reviewed [1]. Most of the work has been directed to the description of the deterministic response to activity and potential changes of ISFETs selective to different kinds of ions. Fluctuation studies on many different electrochemical systems have been reported in the literature. Such studies include redox reactions at metal and semiconductor electrodes [2-5], the dissociation process of beryllium sulfate [6], the nucl[illegible]n and crystal growth of metals and semiconductors and the nucleation of p[illegible]s in lipid bilayers as well as the kinetics of electrocatalysis [7], and the fluctuation

---

Key Words: ISFET, Membrane, Equilibrium, Noise

analysis in biological membranes [8-10] to name only a few. These studies show that the measurement of random electrical fluctuations (commonly referred to as noise) occurring in electrochemical systems can lead to kinetic information, some of which is not accessible by deterministic measurements.

This article presents a study of random fluctuations in the drain current of ISFETs in the range of 1 Hz to 25 kHz for several different ion selective membranes. ISFETs are normally used as potentiometric sensors, which means that no net current flows through the membrane/solution interface. In most ion selective devices the zero net current condition is synonymous with thermodynamic equilibrium. It was, therefore, decided first to investigate the phenomenon in ISFETs in this state. The overall noise exhibited by the drain current of an ISFET is the sum of several contributions. These contributions can be separated as follows:

a. Noise generated in the "solid state" portion of the device which includes thermal noise, generation-recombination noise in the space charge region at the substrate-channel interface, and 1/f noise in the channel [11, 12];

b. Electrochemical noise associated with the ion/membrane interactions which can exhibit thermal noise, shot noise, and 1/f noise;

c. Noise generated in the solution and at the reference electrode, as well as noise resulting from the fluctuations of the biasing elements (power supplies, resistances). The noise spectra for several kinds of ISFETs were measured and interpreted in terms of the electrochemical properties of the membranes.

NOISE CHARACTERIZATION

The drain current $I_D(t)$ in the channel of ISFETs can be expressed by

Equation 1:

$$I_D(t) = \bar{I}_D + i(t) \qquad (1)$$

Where $\bar{I}_D$ is the average value and i(t) is the random fluctuation of the drain current. The random fluctuation or noise i(t) can be quantified and characterized by means of spectral density analysis, correlation analysis and integral spectrum analysis [10, 13, 14]. From an analysis point of view, there is little difference between methods, but there may be some practical difference which favors one or the other in particular circumstances. Furthermore, information obtained with one method can be transformed into information obtained with another method.

For our application, we used spectral density analysis mainly because it is the type of analysis that has been used most often for the measurement of noise in membranes and in electronic devices. In order to define the spectral density of i(t), we use Rayleigh's theorem which states that the area under the square modulus of a function is equal to the area under the square modulus of its Fourier transform. This is represented by Equation 2:

$$\int_{-\infty}^{+\infty} |i(t)|^2 \, dt = \int_{-\infty}^{+\infty} |\bar{i}(f)|^2 \, df \qquad (2)$$

Where $\bar{i}(f)$ is the Fourier transform of i(t) and is by definition given by Equation 3:

$$\bar{i}(f) = \int_{-\infty}^{+\infty} i(t) e^{-j\omega t} \, dt \qquad (3)$$

where $\omega = 2\pi f$, with f being the frequency. Since i(t) is a real signal which exists only for $0 \leq t \leq T$, Rayleigh's theorem can be rewritten as:

$$\int_0^T i^2(t)\, dt = \int_{-\infty}^{+\infty} |\bar{I}(f)|^2\, df \qquad (4)$$

The average value of i(t) is zero and thus, the average value of $i^2(t)$ is the variance σ^2. On the other hand, $|\bar{I}(f)|$ is an even function of frequency which means that the integral over all frequencies may be expressed as twice the integral over the positive frequency axis. So, using Equation 4, we can write:

$$\sigma^2 = \frac{1}{T} \int_0^T i^2(t)\, dt = \frac{2}{T} \int_0^{+\infty} |\bar{I}(f)|^2\, df \qquad (5)$$

By definition, the spectral density $S_i(f)$ of i(t) is given by:

$$S_i(f) = \lim_{T \to \infty} \frac{2}{T} |\bar{I}(f)|^2 \qquad (6)$$

where the subscript i refers to the spectral density of the current.

Combining Equation 5 and 6 leads to:

$$\sigma^2 = \int_0^{+\infty} S_i(f)\, df \qquad (7)$$

This shows that the variance of a signal in a narrow frequency band df is given by $S_i(f)df$ which clarifies the meaning of the spectral density.

If the signal is deterministic and is defined by an analytic expression, the spectral density and the variance are absolutely determined. On the other hand, if the signal is probabilistic, such as random noise, the spectral density and the variance will be different for each time interval T. However, if the random signal is stationary, which means that the variance is

independent of time, the different estimates for spectral density and variance will tend toward a mean value.

There are many experimental ways to estimate the spectral density. The common feature of the different techniques is filtering of the signal. For our measurements, we used a digital spectrum analyzer (HP 3582A) in which the fast Fourier transform (FFT) implements a set of parallel filters digitally and basically calculates the spectral density as a function of the center frequency of the filter. For more information about the characterization and the analysis of noise, see for example, DeFelice [10] or Van der Ziel [13, 14].

EXPERIMENTAL

Devices

The fabrication and modes of operation of ISFETs have been described previously [1]. Basically an ISFET is obtained by replacing the metal gate of the insulated gate field effect transistor (IGFET) with a reference electrode/electrolyte/ion selective membrane electrochemical system.

Figure 1 is a photograph of the integrated circuit we used in our experiments and which has been described in Reference 1. This integrated circuit is composed of two ISFETs (Q_1, Q_3) and two IGFETs (Q_2, Q_4). All devices are n-channel depletion mode field effect transistors.

The devices investigated in this study can be divided into four categories, depending on their gate structure. The first is the standard IGFET structure, which is considered to be the basic device against which ISFET performance is measured. The second is the bare gate silicon nitride ISFET which is known to be pH sensitive [15]. The third group includes ISFETs with

homogeneous polymeric membranes; Ca^{2+}, K^{+}, and Na^{+} selective membranes were used [16-18]. We have also measured ISFETs with gold covered gate which are sensitive to redox couples (redox ISFETs) and which can be operated either as an IGFET or as a redox ISFET.

Power Spectrum Measurements

The experimental arrangement used for electrical noise measurements is shown schematically in Figure 2. The gate bias was provided by a 9 V alkaline cell (Ray-O-Vac No. A1604) appropriately filtered by the low-pass combination R_3 and C in order to avoid possible contamination with battery noise. The -3dB frequency f_{LP} for this low-pass filter is given by Equation 8:

$$f_{LP} = \frac{1}{2 \pi R_3 C} \qquad (8)$$

which with our values gave a frequency of 1.59 Hz. For measurements on ISFETs, the reference electrode used was a custom made Ag/AgCl (saturated KCl) cell of surface area approximately 5 cm^2. The drain bias was such that the devices were operated in the saturation region. The voltage V_2 (Figure 1) consisted of a series combination of four 1.5 V alkaline cells (Duracell MN 1300).

The drain current I_D, which was maintained at 100 μA for all experiments developed a voltage across R_4 (metal film resistor, Dale model RN60D, CMF60D) and the fluctuations of this voltage were amplified using a low noise pre-amplifier (PARC 113). The gain selected for all experiments was 1000 except for amplifier and resistor noise measurements where it was 10,000. The pre-amplifier was ac coupled and its -3dB high frequency roll-off and low frequency roll-off were 300 kHz and 0.03 Hz, respectively. The amplified signal was analyzed using a digital spectrum analyzer (HP 3582A). This instrument has a frequency range of 0.02 Hz to 25 kHz. The combination of the

pre-amplifier, the gate bias low-pass filter and the spectrum analyzer thus allowed us to investigate the frequency range of 1 Hz to 25 kHz.

The IGFET (or ISFET) and its biasing components were enclosed in a Faraday cage to minimize external electrical interference. For each device, spectra were measured in the frequency range 1-10 Hz, 1-100 Hz, 1 Hz - 1 kHz, 1 Hz - 10 kHz and 1 Hz - 25 kHz. Since the measured spectrum is only an estimation of the true spectrum, averaging allows us to improve statistical accuracy and thus to reduce the variance associated with the measured spectrum. So, in each spectral range the power spectrum obtained was the average of N spectra with N = 32. The results reported in this study were collected manually and, of the 256 points available in each spectral range, only a few were collected. The collected points were chosen so that they would be approximately evenly spaced along the frequency axis on a logarithmic scale.

For ISFETs, spectra were measured in 1 mM, 10 mM, and 100 mM aqueous solutions of NaCl, KCl and $CaCl_2$ for Na^+, K^+, and Ca^{2+} ISFETs, respectively. For pH ISFETs, spectra were measured in pH 4, 7, and 10. For these measurements, commercial buffers (VWR Scientific Inc., San Francisco, California 94119) were used. Finally, for redox ISFETs, spectra were measured for different ratios of $[Fe(CN)_6^{4-}]/[Fe(CN)_6^{3-}]$ (0.1, 1, and 10); $[Fe(CN)_6^{4-}]$ being kept constant at 10 mM; these solutions were prepared using $K_4Fe(CN)_6$ and $K_3Fe(CN)_6$ and were buffered at pH 7.2 using 0.1 M H_3PO_4. All chemicals used were of reagent grade. Solutions were prepared with deionized water having a resistivity of 12 to 14 MΩcm. All measurements were conducted at room temperature.

RESULTS AND DISCUSSION

Without any device connected in the system, the experimental arrangement accurately measures the Nyquist noise in the 10 KΩ load resistor, as shown in Figure 3. The amplifier noise was observed to be significantly lower (approximately $5 \cdot 10^{-25}$ A^2/Hz for 10 Hz < f < 25 kHz) than the Nyquist noise in the resistor (the amplifier noise represented here is the output voltage noise spectral density divided by $R_4^2 = 10^8$ Ω^2 for the purpose of comparison with IGFET noise).

Although resistors (especially carbon composition resistors) can exhibit 1/f noise when current flows through them [19], the 10 kΩ load resistor used did not show noise levels larger than the thermal noise when a current of a 100 μA was passed through it, which means that for the frequency range examined and for the particular level of current chosen, the 1/f noise is hidden by thermal noise. The observed noise of all IGFETs and ISFETs examined was several orders of magnitude larger than the amplifier and the load resistor noise level.

Figure 3 also shows the current noise for two geometrically identical IGFETs processed in two different laboratories. The substantially different noise spectra illustrate the dependence of the "integrated circuit" noise on the processing parameters which were different for the two laboratories. This variability in the "integrated circuit" noise was present to a much smaller extent in devices processed in the same laboratory and was undetectable for devices from the same wafer. Spectra (b) and (c) in Figure 3 are most likely a superposition of 1/f noise and generation-recombination (g-r) noise and similar spectra have been reported in the literature [20]; g-r noise may be due to generation-recombination centers in the space charge region existing between the conducting channel and the substrate; on the other hand, 1/f noise may be due to interface states at the Si/SiO_2 interface and to

traps in the SiO_2 [12]. Spectrum (c) in Figure 3 probably indicates a higher concentration of g-r centers in the corresponding IGFETs than in those exhibiting spectrum (b); in addition, the noise levels reported here agree with those reported for metal oxide semiconductor field effect transistors (MOSFETs) by other workers [20, 21].

If device Q_1 or Q_3 (Figure 1) has a gold gate, it can be operated as a regular IGFET by directly biasing the gate or it can be operated as a redox ISFET by biasing the gate through the solution. We observed no difference in the noise levels between these two modes of operation; furthermore, no difference was observed when the concentration of $Fe(CN)_6^{4-}/Fe(CN)_6^{3-}$ redox couple was changed from 0.01 mM to 10 mM at constant ratio of 1:1. The standard rate constant k^o for the charge transfer of our particular couple with gold is on the order of 10^{-2} cms^{-1} [22]. So, this change in concentration corresponds to a change in exchange current density j_o at the gold/solution interface of approximately 10^{-5} A/cm^2 to 10^{-2} A/cm^2 (Equation 9) which in turn corresponds to a variation in low frequency current noise spectral density of about $3 \cdot 10^{-20}$ A^2/Hz to $3 \cdot 10^{-23}$ A^2/Hz, respectively (Equations 10, 11, and 15 and having a gold surface area of $2.3 \cdot 10^{-4}$ cm^2).

$$j_o = \frac{i_o}{A} = nFk^o C_O^{(1-\alpha)} C_R^{\alpha} \qquad (9)$$

where: j_o = exchange current density

i_o = exchange current

A = electrode surface area

n = number of electrons transferred

F = Faraday constant

k^o = standard rate constant

α = transfer coefficient

C_O = bulk concentration of oxidized species

C_R = bulk concentration of reduced species

The relationship between exchange current and noise spectral density will be discussed below. Considering the results shown in Figure 4, we can immediately see that these values are below the "integrated circuit" noise. This means that with our devices, information about the gold/solution interface cannot be obtained from the measurement of equilibrium noise. This, however, is a technological problem and commercially available field effect transistors can reach noise levels as low as 10^{-25} A^2/Hz (for f = 1 Hz) which means that by improved processing leading to a decrease in "integrated circuit" noise we may indeed be able to get information about the gold/solution interface from the measurement of equilibrium noise.

An interesting difference emerged for the noise spectrum of aluminum gate IGFET (Q_2 or Q_4) and gold gate IGFET (gate Q_1 or Q_3 covered with gold). The latter shows higher noise levels at lower frequencies (Figure 4a) than the corresponding aluminum gate IGFET (Figure 4b) on the same chip. This observed additional noise may be explained by additional interface states induced by radiation damage during sputtering of the gold gate [23] which would raise the 1/f noise level.

The interface between silicon nitride (Si_3N_4) and electrolyte contains charge which is pH dependent [1]. Although the exact nature of this charge is not known, ISFETs with Si_3N_4 are used as pH devices which are free from common chemical interference. Their response to steps in applied gate voltage is on the order of a microsecond [24]. We found that the noise spectrum of this device is undistinguishable from the noise of the corresponding IGFET with

aluminum gate. This fact is in agreement with our interpretation of the higher noise levels of the gold gate IGFETs (Q_1 or Q_3). No significant difference in the noise spectrum of pH ISFETs immersed in buffer solutions of pH 4, 7, and 10 was found. As in the case of redox ISFETs, it can be concluded that the equilibrium electrochemical noise is obscured by the "integrated-circuit" noise.

A different situation has been encountered with ISFETs using polymeric ion selective membranes. Noise spectra of Na^+ and K^+ ISFETs are shown in Figure 5, together with the spectrum of pH ISFETs. The polymeric membranes are hydrated which means that the silicon nitride surface under the membrane is also hydrated. From this point of view it is appropriate to subtract the noise spectrum of the pH ISFET from the noise spectra of polymeric membrane ISFETs. Spectra for Na^+ and K^+ ISFETs in Figure 4 were obtained after subtracting the pH ISFET spectrum. For frequencies higher than 100 Hz, K^+ ISFETs did not show noise levels significantly higher than those of pH ISFETs, which is the reason why only points below 100 Hz are shown in this case. Since devices are operated in saturation, current in the 10 kΩ load resistor is effectively the short circuit drain current. Although the noise spectral density is elevated by the presence of polymeric ion selective membranes, no significant variation was observed for different concentrations of the primary ion (1, 10, 100 mM). The noise spectrum of Ca^{2+} ISFETs was only slightly higher that that of the pH ISFET for frequencies larger than 100 Hz and was not included in Figure 5.

Impedance measurements applied to the investigation of ion selective electrodes [25, 26] show that such electrochemical systems can be modeled with equivalent electrical circuits composed of parallel RC combinations in series, each combination corresponding to a specific characteristic of the system. This approach is very important for a better understanding of such systems and is useful in the identification of the parameters limiting the performance of

these systems. In thermodynamic equilibrium, every impedance Z exhibits thermal noise, the voltage spectral density $S_v(f)$ of which is given by the Nyquist equation:

$$S_v(f) = 4\ kT\ Re(Z) \qquad (10)$$

where k = Boltzmann constant

T = absolute temperature

Re(Z) = real part of impedance Z

This is, of course, white noise.

Using computer assisted modeling, we attempted to determine an equivalent electrical circuit for Na^+ and K^+ ISFETs so that the theoretical noise spectra would fit the experimental points as shown in Figure 5. For this task, we used a general purpose circuit simulation program (SPICE) developed by the Computer Sciences Department at the University of California, Berkeley and adapted for use on a HP 3000 computer by the Hewlett-Packard Design Aids Group [27]. Figure 6a shows the electrical equivalent circuit used for modeling. This circuit is comprised of two parts. The first part models the electrochemical system placed over the integrated circuit and is made up of a series of parallel R_jC_j combinations; at this point we do not assign these R_j and C_j elements to any physical part of the electrochemical system; the resistances R_j are generating thermal noise at thermal equilibrium; in our model we represent them as noiseless elements and, in series with them, we place a noise source V_j which has a spectral density given by Equation 10 and which is equivalent to the thermal noise generated across R_j. The second part of the circuit models the integrated circuit and is the simplest equivalent circuit for an IGFET in saturation [28]. In this model C_{GS}

represents the gate to source capacitance, g_m is the transconductance of the device, V_{GS} is the voltage developed across C_{GS}, I_D is the drain current and is equal to $g_m V_{GS}$ and finally R_L is the load resistance (equivalent to R_4 in Figure 2). For our devices, we had $C_{GS} \cong 1.5$ pF and $g_m \cong 4 \cdot 10^{-4}\ \Omega^{-1}$.

It can be safely assumed that the noise sources V_j due to the resistances R_j are uncorrelated. V_j is such that $V_j = (S_{vj}(f))^{1/2}$ and because noise adds by adding spectral densities, we can write for the spectral density $S_i(f)$ of the drain current:

$$S_i(f) = g_m^2 \sum_j V_j^2 \qquad (11)$$

This relationship is exact only at zero frequency but it applies quite well for low frequencies at which filtering due to capacitances C_j and C_{GS} is negligible. Figure 6b schematically shows how the experimental spectrum $S_i(f)$ is taken as being the sum of several contributions $S_{ij}(f)$ due to the thermal noise in R_j. The mathematical expression for the frequency dependence of $S_{ij}(f)$ is very complicated and will not be given here. The values for R_j were obtained by using the expression:

$$R_j = \frac{S_{ij}(0)}{4\ kT\ g_m^2} \qquad (12)$$

which is a combination of Equations 10 and 11. On the other hand initial C_j values were obtained using the approximate expression:

$$S_{ij}(f) \cong \frac{S_{ij}(0)}{1 + \omega^2 R_j^2 (C_j + C_{GS})^2} \qquad (13)$$

This expression allows us to obtain approximate values for C_j from the experimental spectrum. These values are then varied in order to improve the fit of the model with the experimental data. Therefore, using Equation 13 and obtaining the half-power frequency f_j from the experimental spectrum (Figure

6b) we can write:

$$C_j \tilde{=} \frac{1}{2\pi f_j R_j} - C_{GS} \qquad (14)$$

The modeling for a given device is done with a minimal number of RC combinations required to obtain a satisfactory fit. The values which were used to fit the data presented in Figure 5 are shown in Table I. The correlation coefficient r between the model and the experimental data was calculated and we obtained r = 0.9782 for the Na^+ ISFET and r = 0.9980 for the K^+ ISFET. For the K^+ ISFET, the correlation coefficient was calculated for $5 \leq f \leq 100$ Hz, since for frequencies higher than 100 Hz the noise spectral density for this device does not differ from the one for pH ISFETs. As shown in Table I, we have modeled the Na^+ ISFET with three RC combinations; only one RC combination was used for the small frequency range in which the K^+ ISFET can be modeled. Since we observe no changes in noise spectral density when changing the main ion concentration in solution, it must be that the dominant noise is due to a resistance which does not change its value under these conditions. Such a resistance may well be the bulk resistance of the membrane and so, the R_1C_1 combination may be assigned to the bulk properties of the membrane; this applies for both K^+ and Na^+ ISFETs. The R_3C_3 combination observed for the Na^+ ISFETs is most likely associated with the membrane/silicon nitride interface since the time constant $R_3(C_3 + C_{GS}) \tilde{=} 27$ μs is only an order of magnitude larger than the electrical response time of the pH ISFET which has been measured to be on the order of a microsecond [24]. Finally, R_2C_2 may be due to the solution/membrane interface and thus, R_2 would be the charge transfer resistance R_{ct} and C_2 would be the double layer capacitance of this particular

interface. The charge transfer resistance R_{ct} is inversely proportional to the exchange current i_o, as shown by Equation 15:

$$R_{ct} = \frac{RT}{nFi_o} \qquad (15)$$

where R = Molar gas constant

T = absolute temperature

n = number of elementary charges transferred across the interface per elementary event

F = Faraday constant

i_o = exchange current across the interface

R_{ct} should thus change with varation of the exchange current i_o which would lead to a change in the corresponding noise spectral density; according to Equation 9, i_o should change with the ionic activity of the exchanging ion. However, we have mentioned earlier that no change in noise spectral density was observed when varying the solution ionic activity. It is quite conceivable that R_{ct} indeed changes with varying ionic activity but that this change is obscured by the noise of larger magnitude due to the bulk resistance of the membrane. For the Na^+ ISFET the value of R_2 used in Equation 15 leads to an exchange current across the interface of approximately $2 \quad 10^{-10}$ A. The polymeric membranes which were used in this study had poorly defined membrane surface area which makes the interpretation of our results in terms of exchange current density difficult; however, if we consider an area of 1 mm^2 which is a reasonable estimate, it leads to an exchange current density of $2 \quad 10^{-8}$ A/cm^2, which is a rather small value for a nonpolarized interface, considering the solution ionic activities used in our experiments. A study on Na^+ ISFETs [18] reported an electrical response time (response to a voltage step applied to the reference electrode) of approximately 15 ms; τ is the time required to reach 63% of the full response. If we apply a voltage step to

our model for the Na^+ ISFET, we obtain a value of about 0.2 ms for τ. This apparent discrepancy can be explained by considering the simple circuit shown in Figure 7a. R and C represent the impedance of a hypothetical membrane and C_{GS} represents the input capacitance of our integrated circuit, when operated in the saturation mode. If $V_i(t)$ is a step function of amplitude V_O, the time course of the voltage $V_{GS}(t)$ across C_{GS} is given by Equation 16:

$$V_{GS}(t) = V_O \left(1 - \frac{C_{GS}}{C + C_{GS}} \; e^{-t/R(C + C_{GS})}\right) \qquad (16)$$

For $t = 0$, $V_{GS}(0)$ is given by Equation 17,

$$V_{GS}(0) = V_O \; \frac{C}{C + C_{GS}} \qquad (17)$$

This initial fast step is always present in our situation; however, it is only apparent for $C \gtrsim 0.1\ C_{GS}$. After the initial fast step is reached, the response reaches V_O exponentially with a time constant τ^* equal to $R(C + C_{GS})$. If R and C are due only to the geometry of the membrane, even though R and C are geometry dependent, the product RC is indeed geometry independent. However, because of the low C_{GS} values encountered in ISFETs, the condition $C \lesssim 0.1\ C_{GS}$ is not always satisfied and a situation similar to the one illustrated in Figure 7b can arise. The simulation was done for a constant RC product with the ratio $a = C/C_{GS}$ as a parameter. Figure 7b shows the effect of membrane geometry on the electrical response time of the whole system. Returning to the Na^+ device, we can see that the initial fast step is determined by the capacitive divider formed by C_{GS} and the series combination of C_1, C_2, and C_3 (Figure 6a) which according to the values shown in Table I would correspond to an initial step amounting to approximately 42% of the full response and would give a response shape similar to the one for a = 1 in Figure 7b. Because of

differences in the membrane geometry, it may well be that the results presented in Reference 13 have a response shape intermediate between those for a = 0.2 and a = 0.01 in Figure 7b, and thus would show a τ significantly larger than the value presented here. In the case of the K^+ ISFET, we cannot talk about response time values since R_2C_2 and R_3C_3 could not be identified even though they are physically present in the device, and as shown in the case of the Na^+ ISFET, will affect the shape of the response curve.

It has been pointed out [5] that equilibrium noise measurements can give information about the frequency dispersion of the resistive and reactive parts of the equivalent electrical circuit for a system as well as information about the exchange current density at the membrane/solution interface. For metal electrodes, this value can be obtained from Tafel plots, however, for ion selective membranes in which the bulk resistance is comparable to the charge transfer resistance, Tafel plots cannot be obtained and the measurement of equilibrium noise could be the only way to obtain this information. The use of ISFETs is justified because of the wide bandwidth characteristics of these devices and the small surface area of their ion selective membrane. A better definition of membrane geometrical characteristics can be achieved by using suspended mesh ISFETs which were recently developed [29].

The present study has shown two important limitations of the technique. First of all, the "integrated circuit" noise depends strongly on processing. It is not possible to compare directly the noise spectra of devices obtained from different laboratories. Secondly, the "integrated circuit" noise imposes a background level which must be exceeded by the noise of the electrochemical system placed on the integrated circuit in order to extract any information

from it. For example, the noise spectra for Ca^{2+} and to some extent K^+ ISFETs were too close to the noise spectrum of the corresponding pH ISFET in order to obtain kinetic information in the frequency range investigated. Since most ion selective membranes and other nonpolarized electrodes have exchange current densities higher than the values found in this study for the Na^+ ISFET, they probably could not be investigated with this method if the "integrated circuit" noise is not reduced by improved processing. It is, however, possible that noise measurements made on these systems while they are driven out of equilibrium (non-zero net current) will provide additional information about the processes involved at the solution/membrane interface.

ACKNOWLEDGEMENTS

This study was supported by Office of Naval Research. We are grateful to Professors R.P. Buck and R.J. Huber for their helpful and stimulating comments and to Professor W. Simon for donating the Na^+ and Ca^{2+} ionophores. Finally, financial support for one of us (A.H.) was kindly provided by ASULAB S.A., Switzerland.

REFERENCES

1. Janata, J.; Huber, R.J. Ion-Selective Electrode Reviews 1, 31-79, 1979.
2. Tyagai, V.A.; Lukyanchikova, N.B. Surface Science 12, 331-340, 1968.
3. Tyagai, V.A.; Kolbasov, G. Ya. Elektrokhimiya 7, 1722-1725, 1971.
4. Tyagai, V.A. Itagi Nauki Tekh., Electrokhim. 11, 109-175, 1976.
5. Barker, G.C. J. Electroanal. Chem. 21, 127-136, 1969.
6. Feher, G.; Weissman, M. Proc. Nat. Acad. Sci. USA 70, 870-875, 1975.
7. Fleischmann, M.; Labram, M.; Gabrielli, C.; Sattar, A. Surface Science 101, 583-601, 1980.
8. DeFelice, L.J.; Sokol, B.A. Biophys. J. 16, 827-838, 1976.
9. DeFelice, L.J. Int. Rev. Neurobiol. 20, 169-208, 1977.
10. DeFelice, L.J. "Introduction to Membrane Noise," Plenum Press, New York, New York, 1981.
11. Van der Ziel, A.; Chenette, E.R. Adv. Elect. and Electron Phys. 46, 313-383, 1978.
12. Hooge, F.N.; Kleinpenning, T.G.M.; Vandamme, L.K.J. Rep. Prog. Phys. 44, 479-532, 1981.
13. Van der Ziel, A. "Noise: Sources, Characterization, Measurement," Prentice Hall, Inc., Englewood Cliffs, New Jersey, 1970.
14. Van der Ziel, A. "Noise in Measurements," John Wiley and Sons, New York, New York, 1976.
15. Moss, S.D.; Johnson, C.C.; Janata J. IEEE Trans. BME 25, 49-54, 1978.
16. Ammann, D.; Bissig, R.; Guggi, M.; Pretsch, E.; Simon, W.; Borowitz, I.J.; Weiss, L. Helv. Chim. Acta 58, 1535-1548, 1975.
17. McBride, P.T.; Janata, J.; Comte, P.A.; Moss, S.D.; Johnson, C.C.; Anal. Chim. Acta 101, 239-245, 1978.
18. Oesch, U.; Caras, S.; Janata, J. Anal. Chem. 53, 1983-1986, 1981.
19. DeFelice, L.J. J. Appl. Phys. 47, 350-352, 1976.

20. Wu, S.Y. Solid State Electronics 11, 25-32, 1968.

21. Flinn, I.; Bew, G.; Berz, F. Solid State Electronics 10, 833-945, 1967.

22. Marecek, V.; Samec, Z.; Weber, J. J. Electroanal. Chem. 94, 169-185, 1978.

23. Chapman, B. "Glow Discharge Processes," John Wiley and Sons, Inc., New York, New York, 1980.

24. Smith, R.L.; Janata, J.; Huber, R.J. J. Electrochem. Soc. 127, 1599-1603, 1980.

25. Buck, R.P. Hung. Sci. Instrum. 49, 7-23, 1980.

26. Macdonald, J.R. J. Chem. Phys. 61, 3977-3996, 1974.

27. Hewlett-Packard Design Aids, "HPSPICE; User's Manual;" Hewlett-Packard Company, Palo Alto, California, 1980.

28. Senturia, S.D.; Wedlock, B.D. "Electronic Circuits and Applications," John Wiley and Sons, Inc., New York, New York, 1975; Chapter 11.

29. Blackburn, G.F.; Janata, J. J. Electrochem. Soc., 1982, submitted.

FIGURE CAPTIONS

Figure 1. Photograph of integrated circuit showing the two ISFETs (Q_1, Q_3) and the two IGFETs (Q_2, Q_4).

Figure 2. Experimental arrangement for ISFET and IGFET noise measurements (shown with IGFET). Values are: R_1 = 25 kΩ ± 1%; R_2 = 0 - 50 kΩ (potentiometer); R_3 = 100 kΩ ± 1%; R_4 = 10 kΩ ± 1%; C = 1 μF; V_1 = 9 V; V_2 = 6 V.

Figure 3. Noise Spectra.

a) □ : amplifier + resistor noise.

b) 0 : IGFET processed in the HEDCO Laboratory of the University of Utah (average of five measurements).

c) ● : IGFET processed in the microcircuit laboratory of the University of Utah Research Institute (Average of five measurements).

The dotted line indicates the theoretical level for thermal noise in the 10 kΩ resistor. (This level is $1.66 \cdot 10^{-24}$ A^2/Hz at 300°K)

Figure 4. Noise spectra.

a) ● : gold gate IGFET (Q_1 or Q_3) (average of five measurements)

b) O : aluminum gate IGFET (Q_2 or Q_4) on same substrate (average of five measurements)

Figure 5. Noise Spectra.

a) O : pH ISFET (average of five measurements)

b) ● : K^+ ISFET (average of three measurements) pH noise has been subtracted (dotted lines corresponds to model)

c) □ : Na^+ ISFET (average of three measurements) pH noise has been subtracted (solid line corresponds to model)

Figure 6. a) Electrical equivalent circuit used for modeling.

b) schematic explanation of how the experimental spectrum is fit with a sum of individual spectra, each corresponding to a single noise source V_j. (A log-log representation is shown).

Figure 7. a) Circuit showing a hypothetical membrane having an impedance equivalent to R and C in parallel; C_{GS} represents the input capacitance of the integrated circuit.

b) Computer simulated response $V_{GS}(t)/V_0$ for the circuit shown in part (a) for V_i being a voltage step. Simulation is done for RC = constant = 1 ms and for various ratios of $a = C/C_{GS}$; (C_{GS} = constant = 1 pF). τ and τ^* are shown for a = 0.2. τ is measured for the response from the baseline and τ^* is measured for the response from the initial fast step.

TABLE I

Computer Modeling Results for Na^+ and K^+ ISFETs

ISFET	R_1 [MΩ]	C_1 [pF]	R_2 [MΩ]	C_2 [pF]	R_3 [MΩ]	C_3 [pF]
Na^+	1130.0	7.9	113.0	1.6	3.8	5.5
K^+	189.0	26.6	--	--	--	--

R_1C_1 ≡ membrane bulk properties

R_2C_2 ≡ membrane/solution interface

R_3C_3 ≡ membrane/Si_3N_4 interface

(See text)

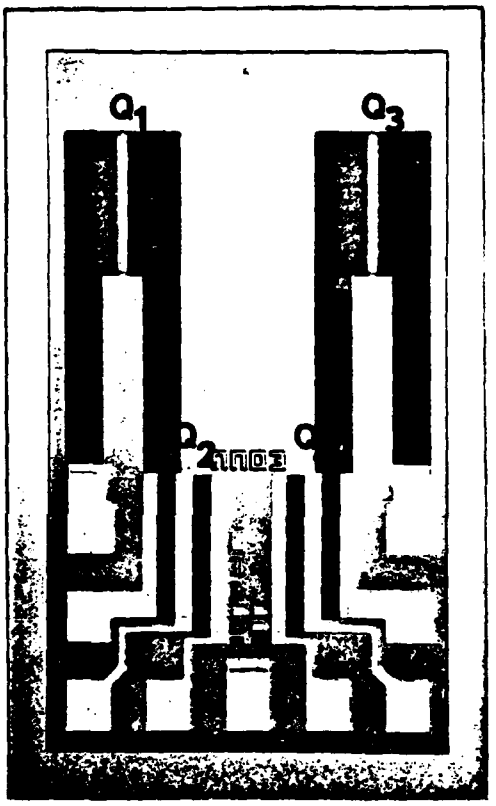

Figure 1

EXPERIMENTAL ARRANGEMENT

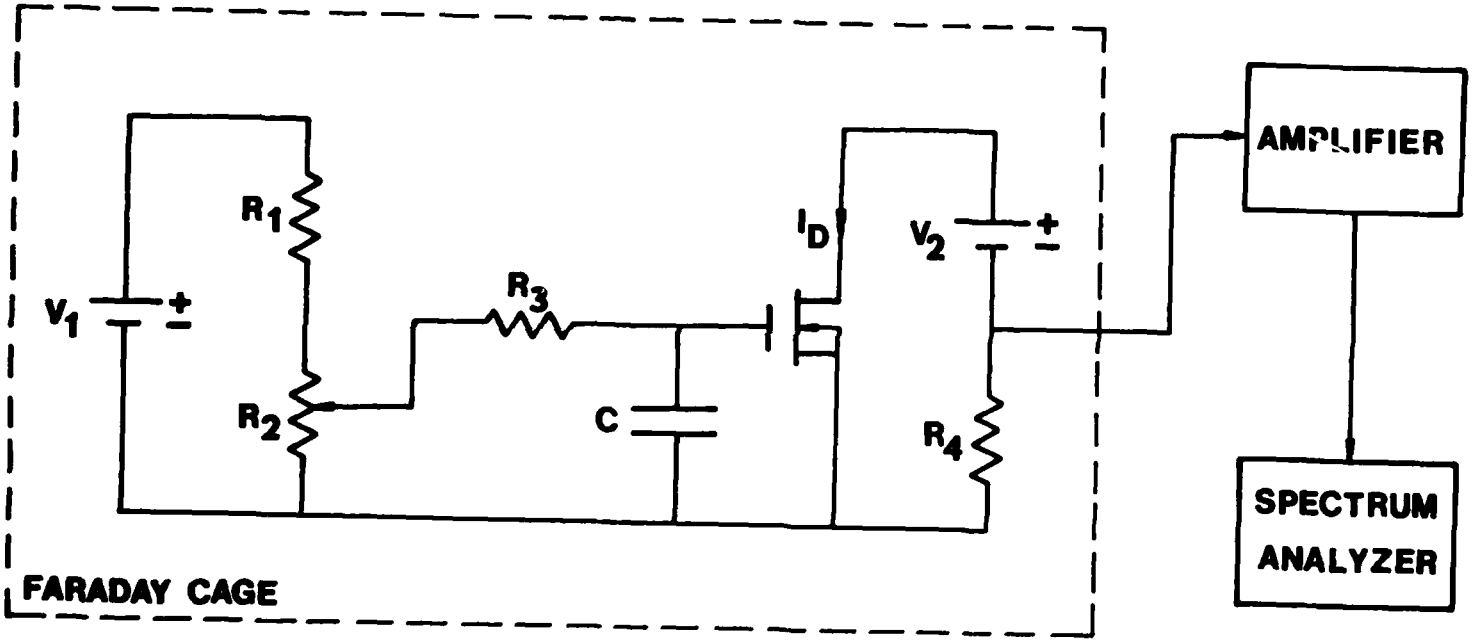

Figure 2

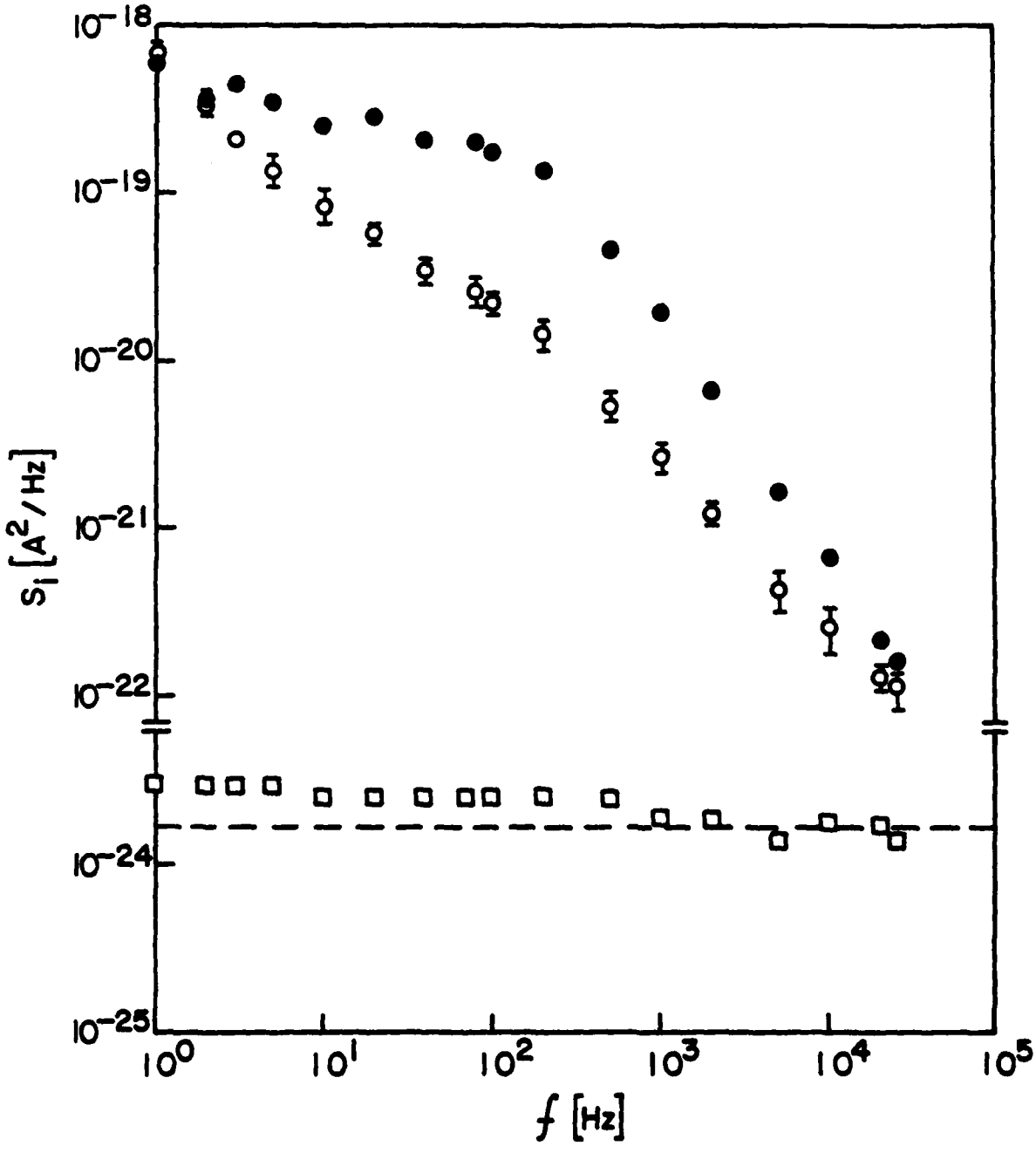
10^{-18}
10^{-19}
10^{-20}
10^{-21}
10^{-22}
10^{-24}
10^{-25}
S_I [A^2/Hz]
10^0
10^1
10^2
10^3
10^4
10^5
f [Hz]

Figure 3

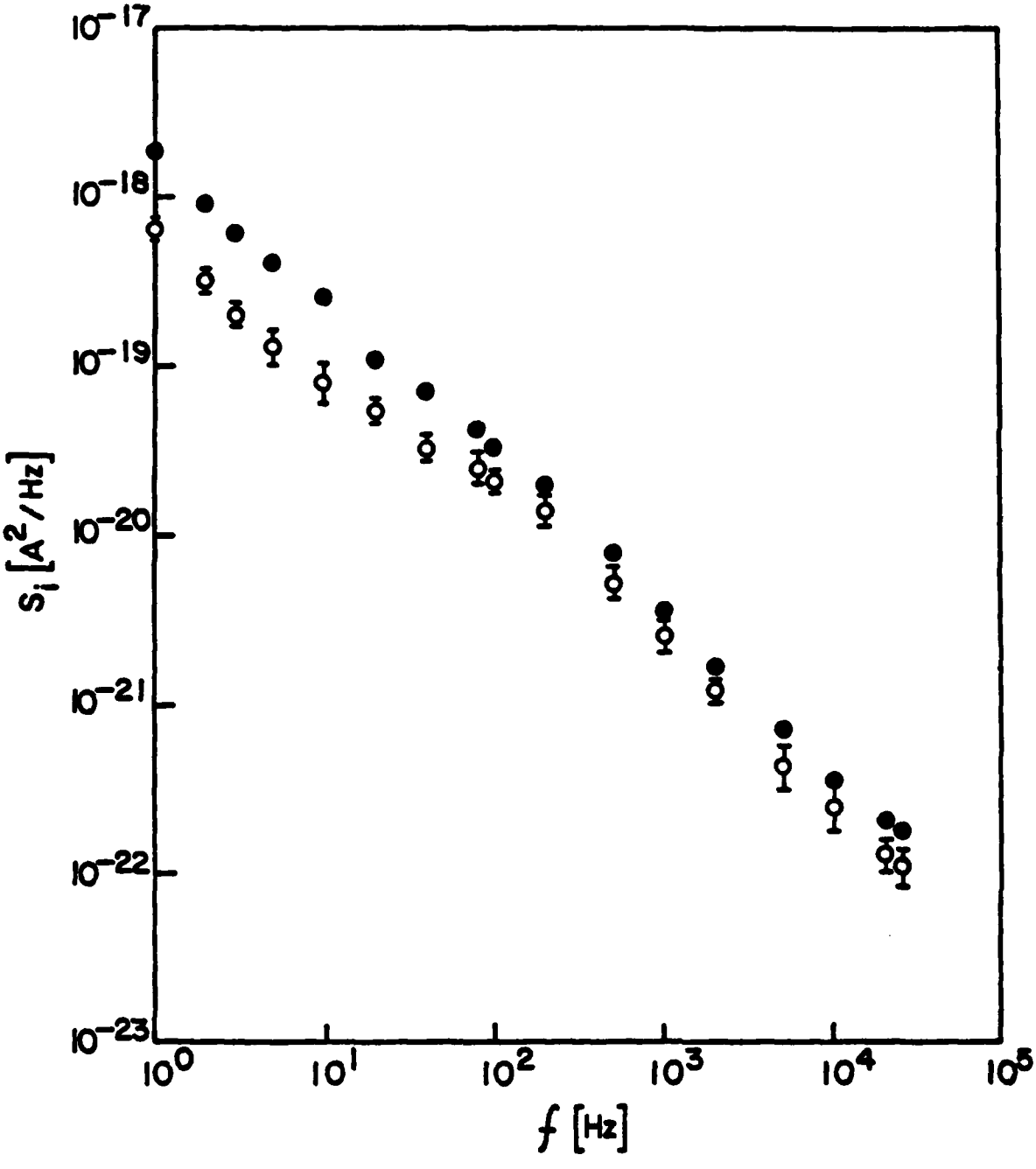
10^{-17}
10^{-18}
10^{-19}
10^{-20}
10^{-21}
10^{-22}
10^{-23}
$S_I\,[A^2/Hz]$
10^0
10^1
10^2
10^3
10^4
10^5
$f\,[Hz]$

Figure 4

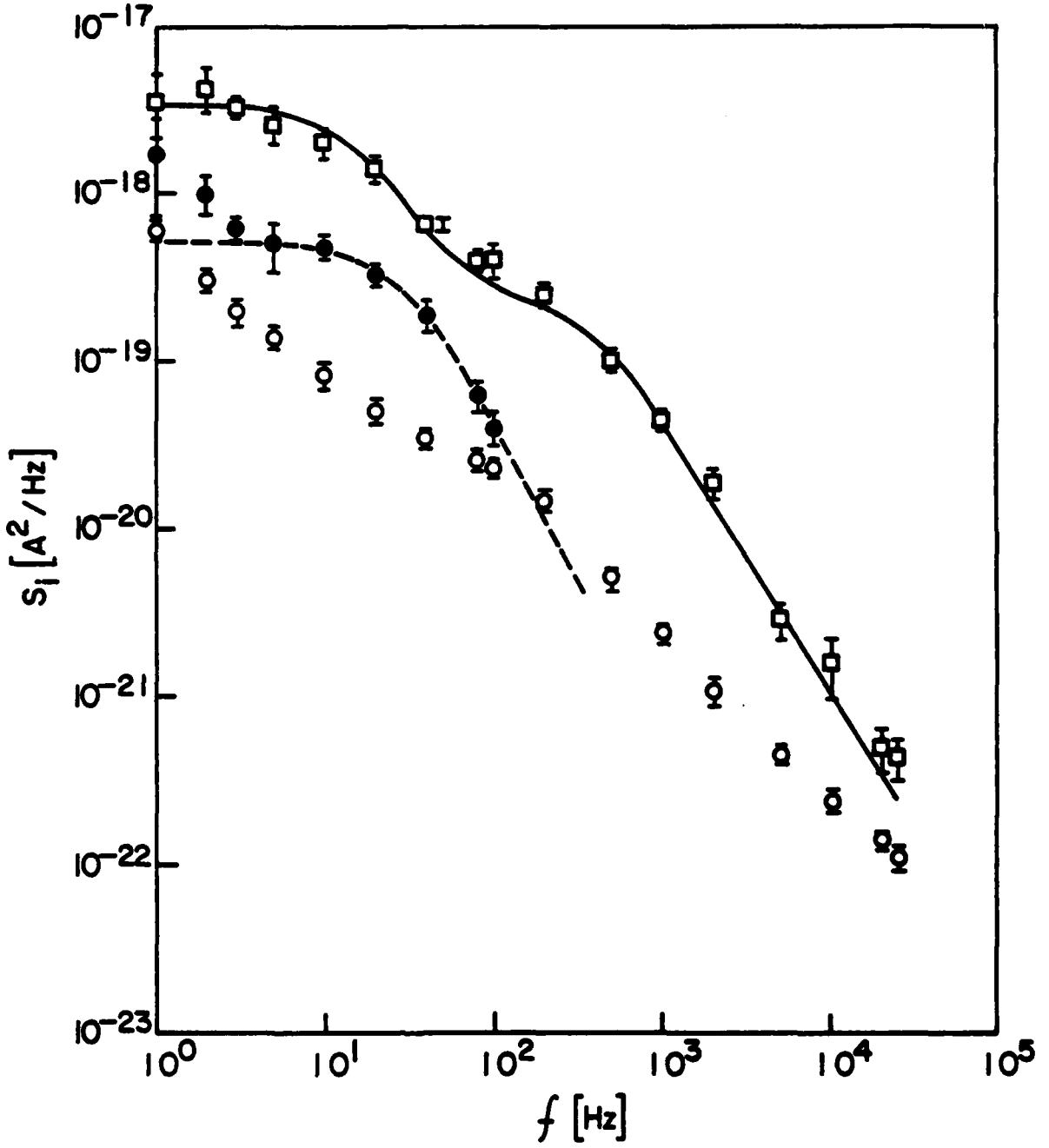
10^{-17}
10^{-18}
10^{-19}
10^{-20}
10^{-21}
10^{-22}
10^{-23}
$S_I [A^2/Hz]$
10^0
10^1
10^2
10^3
10^4
10^5
f [Hz]

Figure 5

NOISE MODELING

A

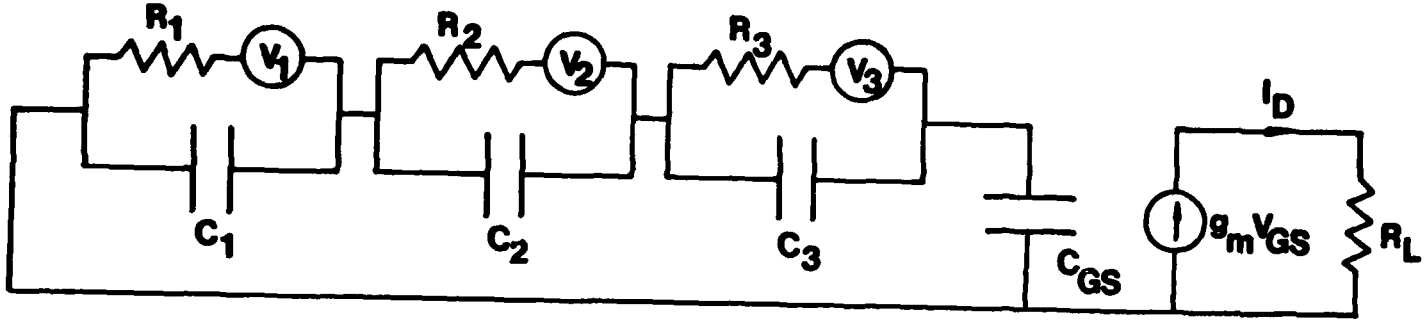

B

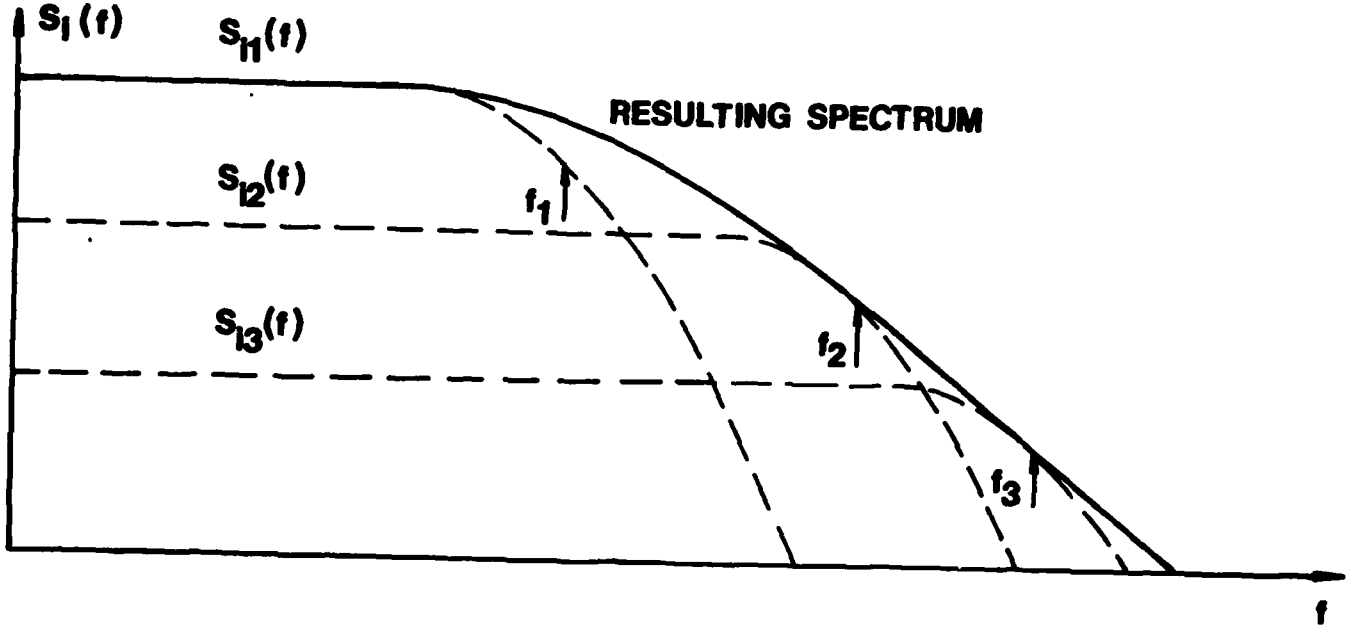

Figure 6

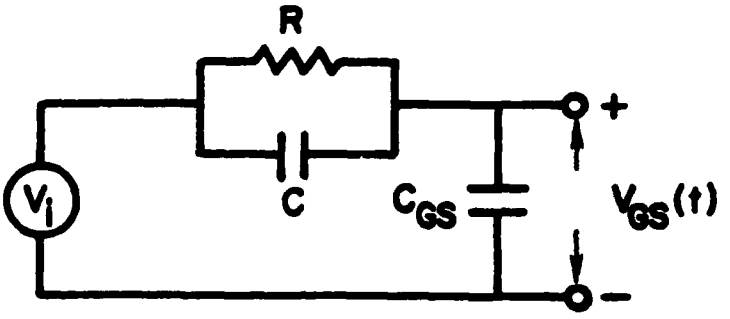
R
C
C_{GS}
V_i
+
−
$V_{GS}(t)$

a.)

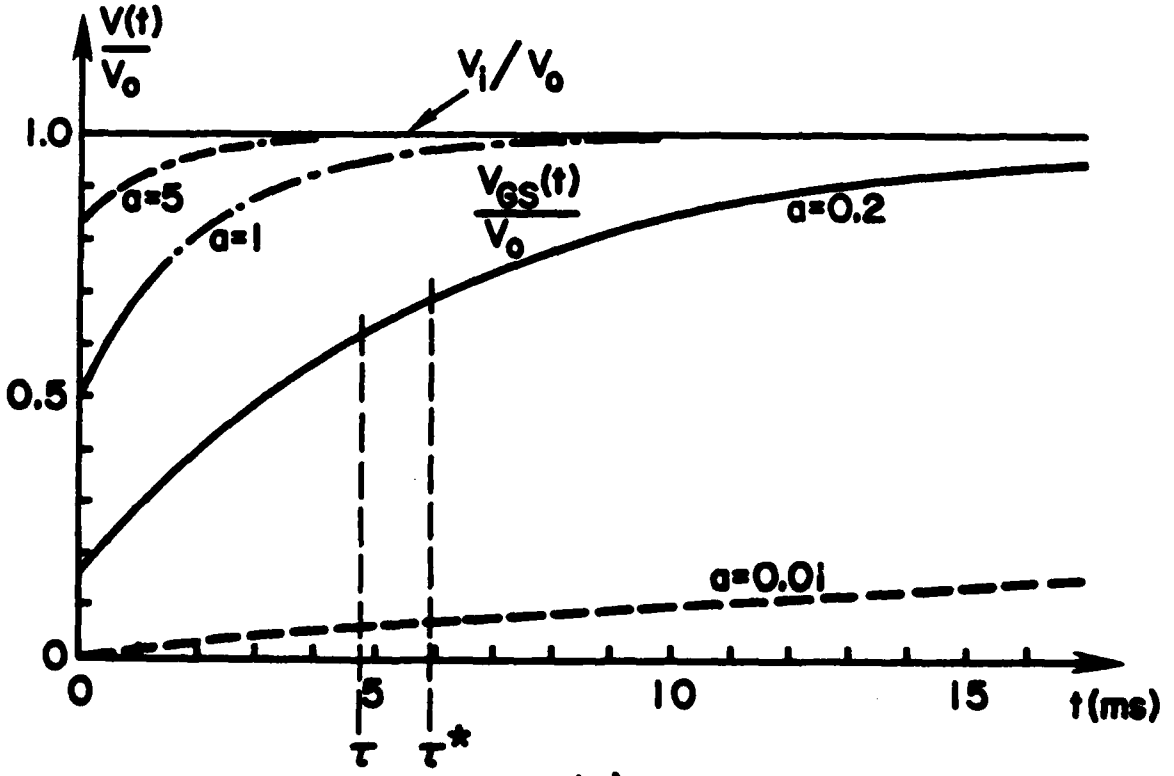
$\frac{V(t)}{V_o}$
V_i/V_o
1.0
0.5
0
a=5
a=1
$\frac{V_{GS}(t)}{V_o}$
a=0.2
a=0.01
0
5
10
15
t(ms)
τ
τ*

b.)

Figure 7

SP472-3/B1

472:GAN:716:lab
78u472-608

TECHNICAL REPORT DISTRIBUTION LIST, 051C

	No. Copies
Dr. M. B. Denton Department of Chemistry University of Arizona Tucson, Arizona 85721	1
Dr. R. A. Osteryoung Department of Chemistry State University of New York at Buffalo Buffalo, New York 14214	1
Dr. B. R. Kowalski Department of Chemistry University of Washington Seattle, Washington 98105	1
Dr. S. P. Perone Department of Chemistry Purdue University Lafayette, Indiana 47907	1
Dr. D. L. Venezky Naval Research Laboratory Code 6130 Washington, D.C. 20375	1
Dr. H. Freiser Department of Chemistry University of Arizona Tuscon, Arizona 85721	
Dr. Fred Saalfeld Naval Research Laboratory Code 6110 Washington, D.C. 20375	1
Dr. H. Chernoff Department of Mathematics Massachusetts Institute of Technology Cambridge, Massachusetts 02139	1
Dr. K. Wilson Department of Chemistry University of California, San Diego La Jolla, California	1
Dr. A. Zirino Naval Undersea Center San Diego, California 92132	1
Dr. John Duffin United States Naval Postgraduate School Monterey, California 93940	1
Dr. G. M. Hieftje Department of Chemistry Indiana University Bloomington, Indiana 47401	1
Dr. Victor L. Rehn Naval Weapons Center Code 3813 China Lake, California 93555	1
Dr. Christie G. Enke Michigan State University Department of Chemistry East Lansing, Michigan 48824	1
Dr. Kent Eisentraut, MBT Air Force Materials Laboratory Wright-Patterson AFE, Ohio 45433	1
Walter G. Cox, Code 3632 Naval Underwater Systems Center Building 148 Newport, Rhode Island 02840	1
Professor Isiah M. Warner Texas A&M University Department of Chemistry College Station, Texas 77840	1
Professor George H. Morrison Cornell University Department of Chemisty Ithaca, New York 14853	1
Professor J. Janata Department of Bioengineering University of Utah Salt Lake City, Utah 84112	1
Dr. Carl Heller Naval Weapons Center China Lake, California 93555	1

TECHNICAL REPORT DISTRIBUTION LIST, 051C

	No. Copies
Dr. L. Jarvis Code 6100 Naval Research Laboratory Washington, D.C. 20375	1

SP472-3/A1

472:GAN:716:enj
78u472-608

TECHNICAL REPORT DISTRIBUTION LIST, GEN

	No. Copies
Office of Naval Research Attn: Code 472 800 North Quincy Street Arlington, Virginia 22217	2
ONR Western Regional Office Attn: Dr. R. J. Marcus 1030 East Green Street Pasadena, California 91106	1
ONR Eastern Regional Office Attn: Dr. L. H. Peebles Building 114, Section D 666 Summer Street Boston, Massachusetts 02210	1
Director, Naval Research Laboratory Attn: Code 6100 Washington, D.C. 20390	1
The Assistant Secretary of the Navy (RE&S) Department of the Navy Room 4E736, Pentagon Washington, D.C. 20350	1
Commander, Naval Air Systems Command Attn: Code 310C (H. Rosenwasser) Department of the Navy Washington, D.C. 20360	1
Defense Technical Information Center Building 5, Cameron Station Alexandria, Virginia 22314	12
Dr. Fred Saalfeld Chemistry Division, Code 6100 Naval Research Laboratory Washington, D.C. 20375	1
U.S. Army Research Office Attn: CRD-AA-IP P.O. Box 1211 Research Triangle Park, N.C. 27709	1
Naval Ocean Systems Center Attn: Mr. Joe McCartney San Diego, California 92152	1
Naval Weapons Center Attn: Dr. A. B. Amster, Chemistry Division China Lake, California 93555	1
Naval Civil Engineering Laboratory Attn: Dr. R. W. Drisko Port Hueneme, California 93401	1
Department of Physics & Chemistry Naval Postgraduate School Monterey, California 93940	1
Scientific Advisor Commandant of the Marine Corps (Code RD-1) Washington, D.C. 20380	1
Naval Ship Research and Development Center Attn: Dr. G. Bosmajian, Applied Chemistry Division Annapolis, Maryland 21401	1
Naval Ocean Systems Center Attn: Dr. S. Yamamoto, Marine Sciences Division San Diego, California 91232	1
Mr. John Boyle Materials Branch Naval Ship Engineering Center Philadelphia, Pennsylvania 19112	1

TECHNICAL REPORT DISTRIBUTION LIST, GEN

	No. Copies
Mr. James Kelley DTNSRDC Code 2803 Annapolis, Maryland 21402	1
Mr. A. M. Anzalone Administrative Librarian PLASTEC/ARRADCOM Bldg 3401 Dover, New Jersey 07801	1